International Journal of Digital Earth

ISSN: 1753-8947 (Print) 1753-8955 (Online) Journal homepage: www.tandfonline.com/journals/tjde20

Predicting bathymetry using multisource differential marine geodetic data with multilayer perceptron neural network

Shuai Zhou, Xin Liu, Yu Sun, Xiaotao Chang, Yongjun Jia, Jinyun Guo & Heping Sun

INTERNATIONAL JOURNAL OF DIGITAL EARTH
2024, VOL. 17, NO. 1, 2393255
https://doi.org/10.1080/17538947.2024.2393255

OPEN ACCESS Check for updates

Predicting bathymetry using multisource differential marine geodetic data with multilayer perceptron neural network

Shuai Zhou[a], Xin Liu[a], Yu Sun[b], Xiaotao Chang[c], Yongjun Jia[d], Jinyun Guo[a] and Heping Sun[e]

[a]College of Geodesy and Geomatics, Shandong University of Science and Technology, Qingdao, People's Republic of China; [b]Key Lab of Spatial Data Mining and Information Sharing of Ministry of Education, Fuzhou University, Fuzhou, People's Republic of China; [c]Land Satellite Remote Sensing Application Center, Ministry of Natural Resources, Beijing, People's Republic of China; [d]National Satellite Ocean Application Service, Ministry of Natural Resources, Beijing, People's Republic of China; [e]State Key Laboratory of Geodesy and Earth's Dynamics, Innovation Academy of Precision Measurement Science and Technology, Chinese Academy of Sciences, Wuhan, People's Republic of China

ABSTRACT

We propose a method for enhancing the accuracy of bathymetry models based on a multilayer perceptron (MLP) neural network that integrates the differences in multisource marine geodetic data (MMGD) (longitude, latitude, reference bathymetry, slope, the meridional and prime components of vertical deflection, gravity anomaly, vertical gravity gradient, and mean dynamic topography). First, we use the MMGD differences between the shipborne sounding control points within $8' \times 8'$ grid points and shipborne sounding control points as input data, as well as the differences between the topo_24.1 model and the measured bathymetric values at the control points as output data to train the MLP model. Second, we feed the input data from the central point of a $1' \times 1'$ grid into the MLP model to obtain predictions, and then use the topo_24.1 model to recover the predicted bathymetry at the prediction point. We focus on the Caribbean Sea, and construct a Caribbean Bathymetric Chart of the Oceans (CBCO1) model using MLP neural network. The reliability of MMGD, a CBCO2 model using MMGD, and the reliability and effectiveness of the overall method are demonstrated through comparisons with the CBCO2, GEBCO_2022, topo_24.1, DTU18 models at the checkpoints.

ARTICLE HISTORY
Received 1 December 2023
Accepted 12 August 2024

KEYWORDS
Multilayer perceptron neural network; multisource marine geodetic data; seafloor topography; Caribbean Sea

1. Introduction

Bathymetric models are essential components of digital elevation models. They are essential in various fields, including marine resource exploration, underwater navigation, seafloor tectonic movement, and marine circulation (Fan et al. 2022; Xu et al. 2022 Yang et al. 2023), and provide fundamental information for geophysical research, geological exploration, and rescue operations (Hsiao et al. 2011; Hu et al. 2021; Polina 2021; Sandwell et al. 2022; Du Toit et al. 2022; Amante et al. 2023; An et al. 2024).

CONTACT Xin Liu xinliu1969@126.com College of Geodesy and Geomatics, Shandong University of Science and Technology, Qingdao 266590, People's Republic of China

different layers are linear; therefore, introducing different activation functions at each layer to enhance the nonlinear characteristics of the MLP neural network is necessary (Figure 1) (Gardner and Dorling 1998).

2.2. Organization of input/output data

The organization of the input and output data directly affects the training accuracy of an MLP model and its ability to accurately predict bathymetry. The bathymetry at a certain point is correlated with surrounding marine gravity data; hence, the MMGD of neighboring grid points are utilized to predict the bathymetry. A greater number of surrounding grid points there are, implies more available information for bathymetry determination. Considering the performance of the computer and the accuracy of the experimental results, an $8' \times 8'$ grid closest to the shipborne bathymetric control point is established, and 64 grid points are selected around the training point. Each grid point is labeled from grid 1 to grid 64, and the input data include relevant information from the surrounding grid points (Figure 1).

In this study, shipborne bathymetric control points are used as training points. The input data used for training are in sequential order as follows: longitude difference (ΔL), latitude difference (ΔB), reference bathymetric difference (Δh), slope difference ($\Delta slope$), the meridional component of vertical deflection difference ($\Delta\xi$), the prime component of vertical deflection difference ($\Delta\eta$), gravity anomaly difference ($\Delta(\Delta g)$), vertical gravity gradient difference (ΔVGG), and mean dynamic topography difference (ΔMDT). The calculation for the input data for training involves the following system of equations:

$$\begin{cases} \Delta L = L^i_{grid} - L_{ip} \\ \Delta B = B^i_{grid} - B_{ip} \\ \Delta h = h^i_{grid} - h_{ip} \\ \Delta slope = slope^i_{grid} - slope_{ip} \\ \Delta\xi = \xi^i_{grid} - \xi_{ip} \\ \Delta\eta = \eta^i_{grid} - \eta_{ip} \\ \Delta(\Delta g) = \Delta g^i_{grid} - \Delta g_{ip} \\ \Delta VGG = VGG^i_{grid} - VGG_{ip} \\ \Delta MDT = MDT^i_{grid} - MDT_{ip} \end{cases} \quad (i = 1, 2 \ldots 64) \tag{1}$$

where i represents the i-th grid point, L^i_{grid} and B^i_{grid} represent the longitude and latitude at the i-th grid point, respectively, and L_{ip} and B_{ip} represent the longitude and latitude at the point of interest for training/prediction, respectively. The variables of h^i_{grid}, ξ^i_{grid}, η^i_{grid}, Δg^i_{grid}, VGG^i_{grid} and MDT^i_{grid} represent the interpolated values of the topo_24.1 model, SIO DOV_32.1 meridional component of the vertical deflection model, SIO DOV_32.1 the prime component of vertical deflection model, SDUST2021GRA model, SIO VGG_32.1 vertical gravity gradient model, and CNES_CLS18 model at the i-th grid point, respectively. Similarly, h_{ip}, ξ_{ip}, η_{ip}, Δg_{ip}, VGG_{ip} and MDT_{ip} represent the interpolated values of these models at the point of interest for training/prediction, respectively. $slope^i_{\mathrm{grid}}$ represents the ratio of the bathymetric difference calculated using the topo_24.1 model at the i-th grid point to the distance, whereas $slope_{ip}$ represents the slope value computed at the point of interest using the topo_24.1 model, where the slope value at a specific point is the average of the slopes in the longitudinal and latitudinal directions (Zhou et al. 2023).

The output data used for training are as follows:

$$\Delta h_{result} = h_{topo\_24.1} - h_{train} \tag{2}$$

where Δh_{result} represents the output data used for the training points, $h_{topo\_24.1}$ represents the bathymetric value of the topo_24.1 model at the training points, and h_{train} represents the measured bathymetric value at the training points.

The points of interest for prediction are located at the center of each $1' \times 1'$ grid within the experimental area. The organization of input data for prediction is the same as that of input data for training, consisting sequentially of the longitude difference (ΔL), latitude difference (ΔB), reference bathymetric difference (Δh), slope difference ($\Delta slope$), the meridional component of vertical deflection difference ($\Delta \xi$), the prime component of vertical deflection difference ($\Delta \eta$), gravity anomaly difference ($\Delta(\Delta g)$), vertical gravity gradient difference (ΔVGG), and mean dynamic topography difference (ΔMDT). Again, the calculation involves the system of equations (1).

Owing to significant differences in the magnitudes of various types of data, it is necessary to standardize both the input and output data to eliminate the influence of different data types on the results:

$$\hat{\mathrm{x}} = \mathrm{x_i} - \bar{x}/\sigma \tag{3}$$

where $\hat{\mathrm{x}}$ represents the standardized data, x_i represents the data before standardization, $\bar{\mathrm{x}}$ represents the mean of the input data, and σ represents the standard deviation (STD) of the input data. After standardization, the mean of the input data becomes zero, and the standard deviation becomes 1.

2.3. Bathymetric inversion process based on the MLP neural network

After determining the input and output data, the MLP model is trained using the following steps (Figure 2).

First, suitable parameters are selected to train the MLP model. Four hidden layers are selected, containing 512, 256, 128, and 64 neurons, respectively. The batch size is set to 16, and the activation function for each layer is the tanh activation function. The loss function used is the mean squared error. During training, the MLP neural network continuously refines its output values to approach the output data. When the loss function no longer decreases, or the maximum number of iterations has been reached, the refinement process terminates. Eventually, through this training process, the MLP model is established.

Second, the input data for the prediction phase are fed into the well-trained MLP model, and the prediction result is obtained. Because the prediction result represents the differences between the bathymetric values from the topo_24.1 model and the bathymetric values at the prediction points, the bathymetric values at the prediction points can be calculated as follows:

$$h_{pred} = \Delta h'_{result} + h'_{topo\_24.1} \tag{4}$$

where h_{pred} represents the bathymetry at point of interest for prediction, $\Delta h'_{result}$ represents the output data in the prediction phase, and $h'_{topo\_24.1}$ represents the bathymetry of the topo_24.1 model at the point of interest for prediction.

Eventually, the CBCO1 model for the experimental area is constructed using the bathymetry values at the prediction points.

2.4. Accuracy evaluation metrics

The coefficient of determination (R^2), mean absolute error (MAE), and standard deviation are used to evaluate the accuracy of both the MLP and the CBCO1 models:

$$R^2 = (1 - (\sum_{j=1}^{n}(h_{0j} - h_j)^2 / \sum_{j=1}^{n}(\bar{h} - h_j)^2)) \times 100\% \tag{5}$$

$$MAE = \sum_{j=1}^{n}|h_{0j} - h_j|/n \tag{6}$$

Figure 6(a) and (b) shows that both the CBCO1 and the CBCO2 models depict variations in seafloor topography within the Caribbean Sea. Figure 6(c) shows the differences between the CBCO1 and CBCO2 models. The differences are primarily close to 0 m, but significant disparities are evident in regions with substantial variations in seafloor topography, such as the Cayman Ridge and the northern part of Young Island.

In this study, a computer equipped with an Intel(R) Core (TM) i5-10400 CPU running at a frequency of 2.90 GHz and 16 GB of memory was used to perform the deep learning workloads. The training process for modeling the CBCO1 model took approximately 12 h, whereas modeling the CBCO2 model required approximately27 h. The time difference during the training phases of the CBCO1 and CBCO2 models was mainly due to discrepancies between the input and output data used for training. These input/output data were fitted more rapidly during training compared to the input/output data used for producing the CBCO2 model. Additionally, fewer iterations were required to find an optimal training structure for the CBCO1, thereby reducing the time cost.

4.2. Model evaluation

The GEBCO_2022 and DTU18 models were used to assess the accuracies of the CBCO1 and CBCO2 models. Using cubic spline interpolation, which is known for its high degree of accuracy and stability, the predicted bathymetries of the CBCO1, CBCO2, GEBCO_2022, topo_24.1, and DTU18 models were obtained at the checkpoints. The differences between the bathymetry predicted by each model and the shipborne bathymetric data were calculated in Area B. Table 1 lists the statistical results.

Table 1 shows that the STD of CBCO1 model is reduced compared to those of the GEBCO_2022, topo_24.1, and DTU18 models by 4.96, 11.16, and 23.08 m, respectively. The STD of the CBCO2 model is reduced compared to those of the topo_24.1 and DTU18 models by 1.89 and 13.81 m, respectively. Based on these indicators, it can be concluded that both the CBCO1 and CBCO2 models exhibit higher accuracies than those of the topo_24.1 and DTU18 models, demonstrating the effectiveness and reliability of the proposed method for modeling seafloor topography. Furthermore, the STD of the CBCO1 model is reduced by 9.29 m compared to that of the CBCO2 model, representing an approximately 10.57% improvement in accuracy; additionally, the MAE is reduced by 4.70 m. These results suggest that differences within the same type of data can have a positive impact on reducing error information, thereby effectively enhancing the accuracy of bathymetric models.

Figure 7 shows the distribution histograms of the differences between the CBCO1, CBCO2, GEBCO_2022, topo_24.1 and DTU18 models and the measured bathymetric values at checkpoints within Area B. Evidently, the errors of all five models follow normal distributions. According to the statistics, the percentages of differences between the five bathymetric models and the measured bathymetry at checkpoints are primarily concentrated within the range of ±200 m (i.e. about twice the STD), i.e. 97.98%, 97.56%, 97.56%, 96.92%, and 97.87%, respectively. Conversely, the percentages of differences greater than ±300 m (i.e. about three times the STD) with respect to the measured bathymetric values are 0.91%, 0.94%, 1.24%, 1.42%, and 1.03%, respectively. In summary, the CBCO1 model exhibits a more concentrated distribution of differences with

Table 1. Statistical results of comparison between CBCO1, CBCO2, GEBCO_2022, topo_24.1, and DTU18 models and measured bathymetric values at checkpoints within the Area B (unit: m).

Model	Max	Min	Mean	STD	RMS	MAE	Correlation coefficient/%
CBCO1	799.25	−807.76	2.54	78.62	78.66	40.40	99.86
CBCO2	1089.70	−1175.60	0.64	87.89	87.89	45.10	99.83
GEBCO_2022	910.23	−1190.00	2.90	83.58	83.63	40.92	99.84
topo_24.1	541.68	−542.90	4.26	89.78	89.88	46.70	99.83
DTU18	2190.40	−2482.90	−1.68	101.70	101.71	44.67	99.77

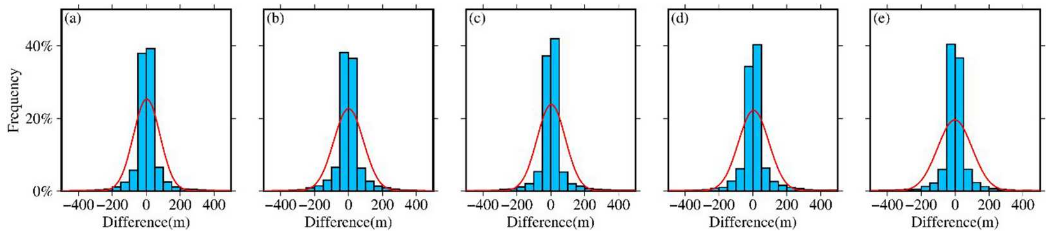

Figure 7. Histograms of the distribution of the differences between each bathymetric model and the measured bathymetric values at checkpoints, with the red line representing the normal distribution curve. (a) CBCO1 model, (b) CBCO2 model, (c) GEBCO_2022 model, (d) topo_24.1 model, (e) DTU18 model.

Table 2. Statistics of the differences for CBCO1, CBCO2, GEBCO_2022, topo_24.1, DTU18 models under different depths at the checkpoints (unit: m).

Different depths	Number of check points	Model	Mean	STD	MAE
(0,1000)	1047	CBCO1	−7.37	67.13	33.93
		CBCO2	−13.52	88.01	40.07
		GEBCO_2022	−3.29	72.80	35.25
		topo_24.1	−8.74	76.30	37.10
		DTU18	−10.58	78.19	33.95
[1000,2000)	2744	CBCO1	−6.34	68.76	36.62
		CBCO2	−5.11	75.79	41.56
		GEBCO_2022	−9.20	74.43	36.88
		topo_24.1	−10.71	76.48	38.53
		DTU18	−7.28	70.33	36.59
[2000,3000)	1722	CBCO1	1.93	96.80	54.89
		CBCO2	5.59	105.34	61.24
		GEBCO_2022	−2.91	102.07	54.88
		topo_24.1	−5.97	103.73	59.65
		DTU18	−3.30	107.69	56.46
[3000,4000)	2839	CBCO1	−4.60	91.66	48.89
		CBCO2	−1.83	102.13	54.63
		GEBCO_2022	−6.82	92.34	48.96
		topo_24.1	−5.97	102.64	56.65
		DTU18	2.39	125.04	59.86
[4000,+∞)	6261	CBCO1	−0.36	72.08	35.30
		CBCO2	2.29	79.90	38.74
		GEBCO_2022	1.71	78.86	37.02
		topo_24.1	−7.71	86.52	43.79
		DTU18	8.71	102.75	40.05

respect to the measured bathymetric values, indicating its ability to better reflect seafloor topography information.

The performances of the five models at the checkpoints under different water depths are listed in Table 2. Evidently, the accuracy of the CBCO1 model is superior to those of the CBCO2, GEBCO_2022, topo_24.1, and DTU18 models across different water depth ranges. This suggests that the CBCO1 model is suitable for a wide range of water depths.

5. Conclusion

This study proposed a method for creating a bathymetric model using a MLP neural network. This method utilized the differences in MMGD between grid points and points of interest to create a bathymetric model with a grid resolution of 1′×1′ for the Caribbean Sea (17-22°N, 271-280°W), referred to as the CBCO1 model. The MMGD included longitude, latitude, reference depth, slope, the meridional and prime components of vertical deflection, gravity anomaly, vertical gravity